Search for $t\bar{t}$ resonances in ATLAS Data

Hamza and Hassan

Advanced Laboratory Course: Particle Physics
Instructor: Dr. Salvatore La Cagina

Department of Physics
TU Dortmund

June 21, 2025

Abstract

This report describes a search for a hypothetical heavy neutral resonance, denoted Z', decaying to top–antitop ($t\bar{t}$) pairs using proton–proton collision data recorded by the ATLAS detector at $\sqrt{s} = 13\,\text{TeV}$, corresponding to an integrated luminosity of $1\,\text{fb}^{-1}$. Events in the lepton+jets final state were selected by requiring exactly one high-p_T electron or muon, at least four jets (two b-tagged), and significant missing transverse momentum. Basic "low-level" observables such as individual object p_T spectra were found to have limited discrimination power, motivating the use of "high-level" variables—most notably the reconstructed $t\bar{t}$ invariant mass $m_{t\bar{t}}$—as the final discriminant. Monte Carlo simulations of Standard Model backgrounds ($t\bar{t}$, W/Z+jets, single top, diboson) were normalized to theory cross sections and compared to data in control regions, demonstrating good agreement. A binned χ^2 test of the $m_{t\bar{t}}$ spectrum showed no significant deviation from the background-only hypothesis. In the absence of a signal, 95% confidence-level upper limits on $\sigma(pp \to Z') \times \mathcal{B}(Z' \to t\bar{t})$ were derived as a function of $m_{Z'}$, excluding production rates above a few picobarns for masses up to several TeV. This exercise illustrates the workflow of a modern high-energy physics analysis, from data preparation and object reconstruction through statistical interpretation.

Contents

1 Introduction

The pursuit of physics beyond the Standard Model (SM) is a central objective of the Large Hadron Collider (LHC) program. Many SM extensions predict a heavy neutral gauge boson, commonly denoted Z, which can couple preferentially to third-generation quarks and decay into a top–antitop ($t\bar{t}$) pair. This report describes an analysis of proton–proton collision data recorded by the ATLAS detector at $\sqrt{s} = 13\,\text{TeV}$, corresponding to an integrated luminosity of $1\,\text{fb}^{-1}$. The analysis searches for a narrow Z resonance by looking for a localized excess in the reconstructed $t\bar{t}$ invariant-mass spectrum. The workflow follows a typical high-energy physics measurement: data retrieval, object reconstruction, event selection, definition of a final discriminant, and a statistical test to assess any potential signal above SM backgrounds.

After this overview, Section 1.1 briefly describes the ATLAS detector, emphasizing the subsystems most relevant to reconstructing top-quark decay products. Section 1.2 outlines the specific task of this study: searching for $Z \to t\bar{t}$ in the lepton+jets channel, including object definitions, event selection, and statistical interpretation.

1.1 The ATLAS Detector

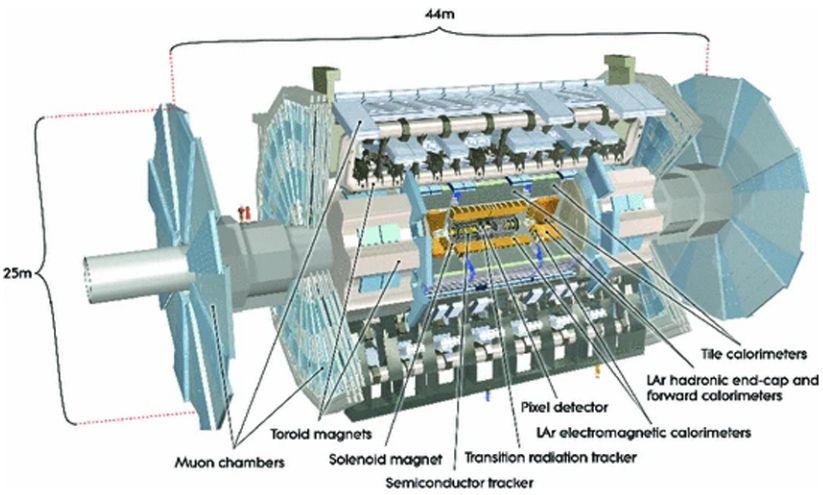

Figure 1: Schematic of the ATLAS detector.

ATLAS is a multipurpose detector covering nearly the full solid angle around the interaction point as shown in Figure 1. From the beam pipe outward, it consists of:

- **Inner Detector (ID)**: Operating inside a 2 T solenoidal magnetic field, the ID combines three subsystems—silicon pixel layers, silicon microstrip layers (SCT), and a transition radiation tracker (TRT). Together, they provide precision tracking for $|\eta| < 2.5$ and excellent vertex resolution for b-tagging.

- **Calorimeters**: A lead–liquid-argon electromagnetic calorimeter (EMCal) covers $|\eta| < 3.2$ and a steel–scintillator tile calorimeter (HCal) covers $|\eta| < 1.7$, supplemented by LAr hadronic endcaps and forward calorimeters to extend coverage to $|\eta| < 4.9$. These measure the energies of electrons, photons, and jets, and provide the missing transverse momentum (E_T^{miss}) essential for identifying neutrinos.

- **Muon Spectrometer (MS)**: Encompassing large air-core toroidal magnets, the MS reconstructs muons in $|\eta| < 2.7$. Drift tubes and cathode strip chambers serve as precision trackers, while resistive plate chambers and thin gap chambers provide a fast Level-1 muon trigger.

- **Trigger and DAQ**: A two-level trigger reduces the 40 MHz collision rate to $\mathcal{O}(1\,kHz)$ for storage. A hardware-based Level-1 trigger uses coarse calorimeter and muon information, followed by a software-based High-Level Trigger that applies near-offline reconstruction for electrons, muons, jets, and E_T^{miss}.

The combination of precise tracking, fine-granularity calorimetry, and an efficient muon system allows ATLAS to identify electrons (up to $|\eta| < 2.47$), muons (up to $|\eta| < 2.7$), jets (up to $|\eta| < 4.5$), and b-tagged jets, as well as to measure E_T^{miss} reliably. These capabilities are crucial for reconstructing $t\bar{t}$ events in the lepton+jets final state.

1.2 Analysis Task: Searching for Z→$t\bar{t}$ in the Lepton+Jets Channel

The goal of this analysis is to search for a spin-1 Z resonance, with mass m_Z in the range 500 GeV to 3 TeV, decaying into $t\bar{t}$. Since each top quark decays almost exclusively via $t \to Wb$, and each W can decay either leptonically ($W \to \ell\nu$, $\ell = e, \mu$) or hadronically ($W \to q\bar{q}'$), $t\bar{t}$ final states are classified as:

- **All-hadronic**: Six jets, including two b-jets.

- **Lepton+jets**: One charged lepton, one neutrino (E_T^{miss}), and four or more jets (two b-tagged).

- **Dileptonic**: Two leptons, two neutrinos (E_T^{miss}), and two b-jets.

This analysis focuses on the lepton+jets channel, which balances a reasonable signal branching fraction (approximately 30% when including both e and μ) with manageable backgrounds and the advantage of a single-lepton trigger.

Data and Simulation Samples The data consist of pp collisions recorded in 2016 at $\sqrt{s} = 13\,\text{TeV}$, corresponding to $1\,\text{fb}^{-1}$. Events must satisfy a single-lepton trigger: $E_T > 25\,\text{GeV}$ for electrons or $p_T > 25\,\text{GeV}$ for muons. Monte Carlo simulations include:

- **SM $t\bar{t}$ background**: Generated at NLO+parton shower, normalized to NNLO+NNLL cross sections.

- **Subleading backgrounds**: Single-top, W+jets, Z+jets, and diboson (WW, WZ, ZZ), each normalized to the best theoretical cross sections.

- **Z Signal**: Benchmark masses $m_Z = 500$, 700, 1000, 1500, 2000, 3000 GeV, with a narrow width ($\Gamma/m \sim 1\%$) and SM-like couplings to $t\bar{t}$. Full detector simulation is applied to all samples.

Object Reconstruction

- **Leptons:** Electrons are reconstructed from EMCal clusters matched to ID tracks, required to pass "Tight" identification, $E_T > 25\,\text{GeV}$, $|\eta| < 2.47$ (excluding $1.37 < |\eta| < 1.52$), and an isolation criterion ($p_T^{\text{cone30}}/p_T < 0.06$). Muons are "combined" ID+MS tracks with "Medium" identification, $p_T > 25\,\text{GeV}$, $|\eta| < 2.5$, and isolation ($\sum p_T^{\text{tracks}}/p_T < 0.06$).
- **Jets and b-Tagging:** Jets are clustered with the anti-k_t algorithm ($R = 0.4$) from calibrated topological clusters. Jets must satisfy $p_T > 25\,\text{GeV}$, $|\eta| < 2.5$, and standard quality criteria. A multivariate b-tagging algorithm (MV2c10) at the 70% efficiency point identifies b-jets.
- **Missing Transverse Momentum (E_T^{miss}):** Computed as the negative vector sum of calibrated lepton and jet momenta plus a "soft term" for low-p_T tracks, with a requirement $E_T^{\text{miss}} > 20\,\text{GeV}$ to ensure reliable neutrino reconstruction.

Event Selection Events must contain exactly one isolated lepton (e or μ) with $p_T > 25\,\text{GeV}$, at least four jets with $p_T > 25\,\text{GeV}$ (two of which are b-tagged), and no additional leptons. The transverse mass of the W boson,

$$m_T(W) \;=\; \sqrt{2\,p_T^{\ell}\,E_T^{\text{miss}}(1-\cos\Delta\phi(\ell, E_T^{\text{miss}}))},$$

is required to exceed 30 GeV, reducing multijet background. Top-quark reconstruction proceeds as follows:

1. **Hadronic top (t_{had}):** Select three jets (one b-tagged) whose invariant mass best matches the top-quark mass ($\sim 172\,\text{GeV}$).
2. **Leptonic top (t_{lep}):** Combine the isolated lepton, E_T^{miss} (as the neutrino), and one b-tagged jet. Impose $m(\ell\nu) = 80.4\,\text{GeV}$ to solve for the neutrino's longitudinal momentum. Events without a real solution or with poorly reconstructed masses are discarded.

Final Discriminant The key variable is the invariant mass of the reconstructed $t\bar{t}$ system,

$$m_{t\bar{t}} \;=\; m(p_{t_{\text{had}}} + p_{t_{\text{lep}}}).$$

In the absence of a Z, the SM background yields a smoothly falling $m_{t\bar{t}}$ distribution. A narrow Z would appear as a localized bump. Additional kinematic variables (e.g., $\Delta R(\ell, j)$, top p_T, $t\bar{t}$ pseudorapidity) are used to validate modeling and optimize selection.

Statistical Interpretation A binned likelihood fit compares the observed $m_{t\bar{t}}$ spectrum to the sum of SM background templates (dominantly $t\bar{t}$, plus single-top, W+jets, Z+jets, and diboson). Systematic uncertainties—integrated luminosity (4%), jet energy scale and resolution, b-tagging efficiency, lepton efficiencies (2–3%), and theoretical cross sections (10–15%)—are treated as nuisance parameters affecting both normalization and shape. If no significant excess is observed, 95% confidence-level upper limits on $\sigma(pp \to Z) \times \mathcal{B}(Z \to t\bar{t})$ are derived as a function of m_Z using the CL_s method. These limits are compared to benchmark theoretical models (e.g., a Sequential SM Z) to set lower bounds on m_Z.

In summary, this analysis uses ATLAS's tracking, calorimetry, and muon systems to reconstruct $t\bar{t}$ candidates in the lepton+jets channel and search for a narrow Z resonance. The structure of the remainder of this report follows a standard ATLAS publication.

2 Data Analysis

In this section, we will describe in detail, the motivation and techniques used to apply the cuts, creating high level observables, selecting the most discriminatory variables and finally making a statistical inference.

2.1 Applying cuts

In section 1.2 a detailed description of the available data and monte-carlo simulations is provided.To isolate the $\rightarrow t\bar{t}$ signal in the lepton+jets channel and suppress SM backgrounds, a sequence of selection criteria is applied in `runSelection.C`. The executable is run via:

```
./runSelection.exe <input file>
```

Each cut's efficiency is monitored and the cumulative acceptance×efficiency ($A \cdot \epsilon$) is printed after every step. The cumulative efficiency is the ratio of the number of events in the sample after the cut to that before the cut is applied. We want to maximize the efficiency for the Z' simulation samples and minimize it for the background samples such as $t\bar{t}$, W, di-boson, etc.

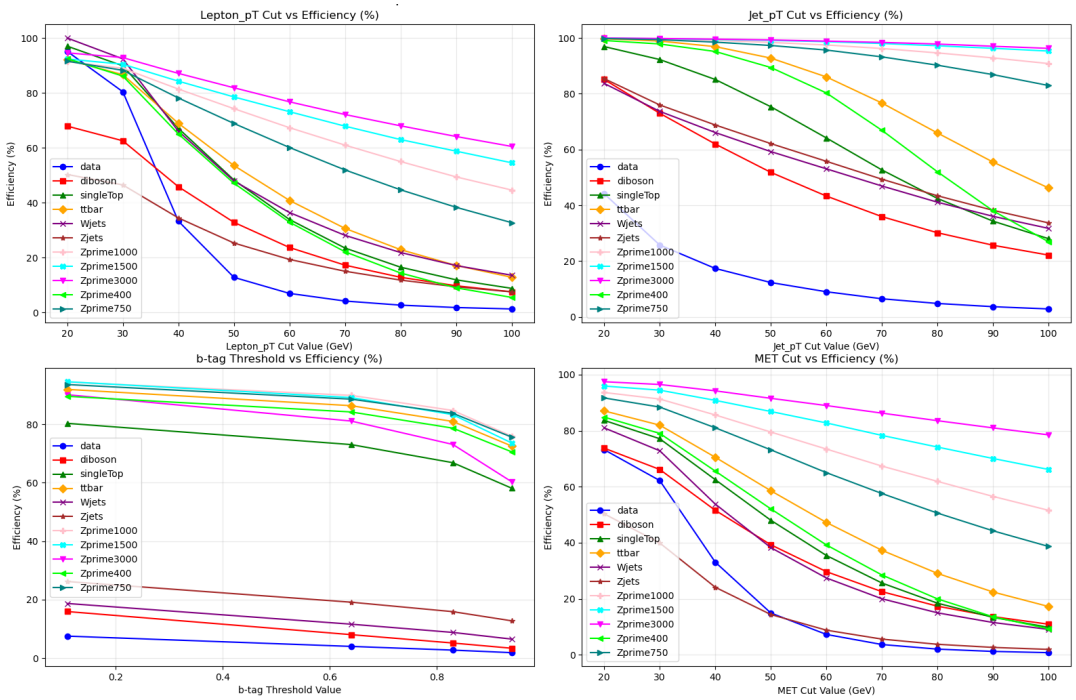

Figure 2: Efficiency plots for the various observables

From figure 2, we can see that the transverse momentum of the highest p_t-jet has quite a high impact on the efficiency, then comes the lepton p_t and the missing energy. b-tag threshold does not impact significantly the efficiency.

Upon inspection of the efficiency and discussion with the lab instructor, the following cuts were agreed upon:

- **No. of Leptons = 1:** Since we are studying 1 lepton events, it is obvious to have this selection criteria.
- **Lepton p_t > 50 GeV** From the efficiency graphs we see that this condition has a fairly high drop in the background efficiency and no so much on the signal.
- **p_t of at least one jet > 80 Gev:** This is similarly decided from the efficiency plot.
- **Number of jets between 3 and 5:** Since we are studying 4-jet events, it seems justifiable to restrict the events to those that have jets between 3 and 5 after accounting for any jet miscountings.
- **$b-$tag threshold:** The $b-$tag threshold was kept at 0.83 as was suggested in the instructions.

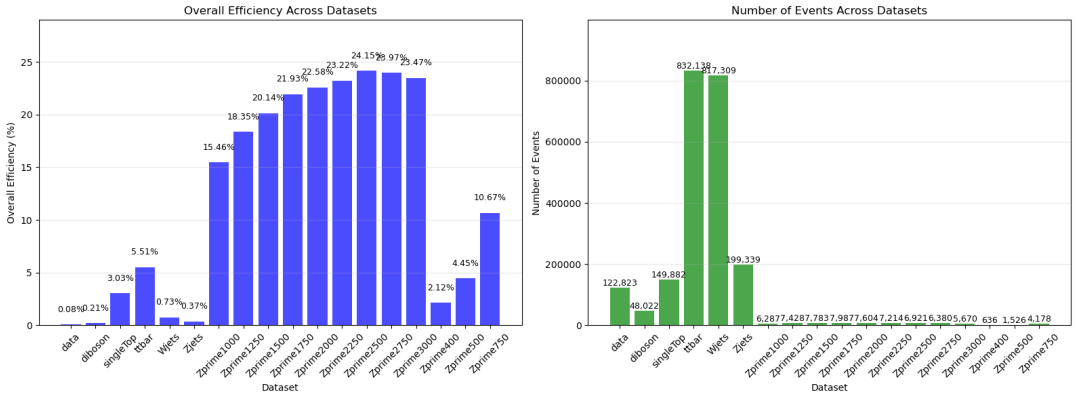

Figure 3: Overall result of the cuts on all samples

In figure 3, we see the overall effect on the efficiency after applying said cuts. We see that the efficiency of background samples has been reduced pretty heavily as compared to that of the signal samples. The main background process is $t\bar{t}$ decays. Unfortunately, our data sample has been cut pretty harshly too which is an early sign that our hypothetical particle is not there in Mother Nature.

2.2 Discriminatory Observables

In order to separate a potential $Z' \to t\bar{t}$ signal from Standard Model backgrounds, we study various kinematic quantities—*discriminatory observables*—that exhibit different shapes for signal and background. These observables fall into two classes:

2.2.1 Low-Level Observables

Low-level observables are basic quantities associated with individual reconstructed objects (leptons, jets, E_T^{miss}, etc.). Examples include:

- Transverse momentum p_T of the leading and subleading jets or leptons,
- Jet multiplicity (≥ 1, ≥ 2, ≥ 3 jets, ...),
- Missing transverse energy E_T^{miss},
- Transverse Momentum of Lepton, etc.

Because they depend on single objects, low-level observables are often *only mildly* sensitive to the heavy resonance mass. For instance, Figure 4 shows the p_T distribution of the leading jet for SM $t\bar{t}$ background and for a Z' signal with $m_{Z'} = 1000\,\text{GeV}$. Although the signal exhibits a slightly harder spectrum, the overlap with background is large. Any cut on a single-object p_T would either leave too much background (if loose) or sacrifice a large fraction of signal (if tight).

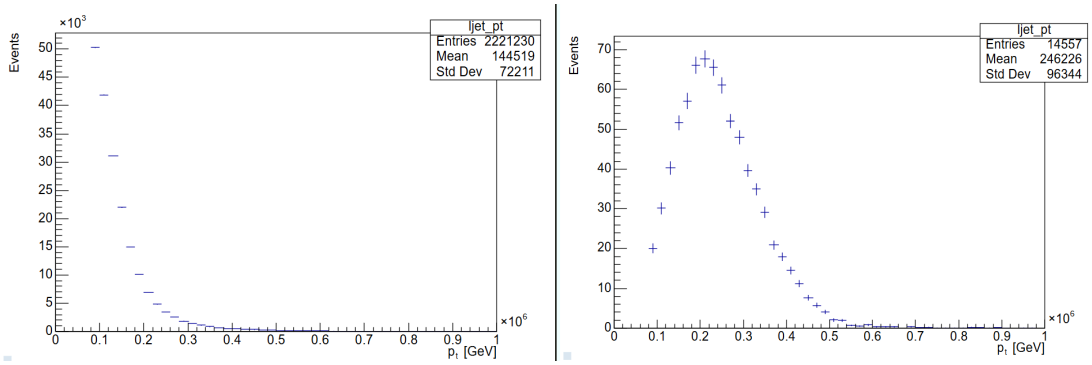

Figure 4: Leading-jet transverse momentum for SM $t\bar{t}$ (left) and Z' ($m_{Z'} = 1000\text{GeV}$, right). The shaded regions indicate the typical cut thresholds.

Similar studies of lepton p_T, jet multiplicity, and simple angular variables yielded only modest discrimination power. Consequently, low-level observables alone cannot serve as the final discriminant in a resonance search.

Note: The highest jet transverse momentum was just chosen as an example to show that the low-level observables do not have much discriminatory power. We think it'll be fruitless to include figures of all the low-level observables that were plotted during the actual analysis because the conclusion remains unchanged.

2.2.2 High-Level Observables

High-level observables combine information from multiple reconstructed objects to exploit the event topology characteristic of heavy resonances. By correlating kinematics across jets, leptons, and E_T^{miss}, these variables can amplify the differences between signal and background. Examples include:

- Invariant mass of object combinations (e.g. three jets for the hadronic top, or the full $t\bar{t}$ system),
- the pseudorapidity of the system formed by the four jets with largest pT, the lepton and the neutrino,
- Angular correlations such as $\Delta R(\ell, b)$ between the lepton and the closest b-jet.

The most powerful high-level variable for a narrow Z' resonance is the invariant mass of the reconstructed $t\bar{t}$ system:

$$m_{t\bar{t}} \;=\; m(p_{t_{\mathrm{had}}} + p_{t_{\mathrm{lep}}}),$$

where t_{had} is built from three jets (one b-tagged) and t_{lep} from the lepton, E_T^{miss} (as the neutrino), and one b-tagged jet. Figure 5 displays the $m_{t\bar{t}}$ spectrum for SM $t\bar{t}$ and for a Z' with $m_{Z'} = 1000\,\mathrm{GeV}$. The signal appears as a narrow peak at 1TeV, whereas the background falls smoothly, yielding a clear separation.

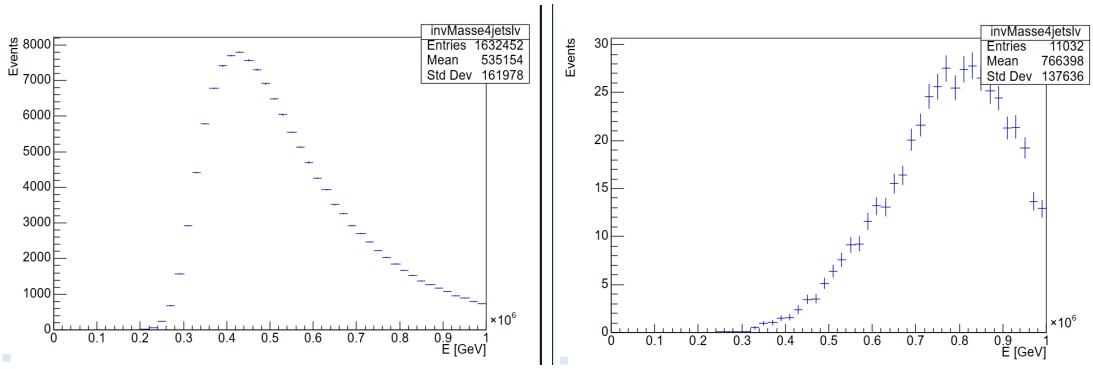

Figure 5: Reconstructed $t\bar{t}$ invariant mass for SM $t\bar{t}$ (left) and Z' signal ($m_{Z'} = 1000\,\mathrm{GeV}$, right).

Because of its superior discrimination, $m_{t\bar{t}}$ is chosen as the final discriminant in the statistical analysis. Other high-level variables are used to validate reconstruction quality and control systematic uncertainties, but the invariant-mass peak remains the most sensitive signature of a narrow Z' resonance.

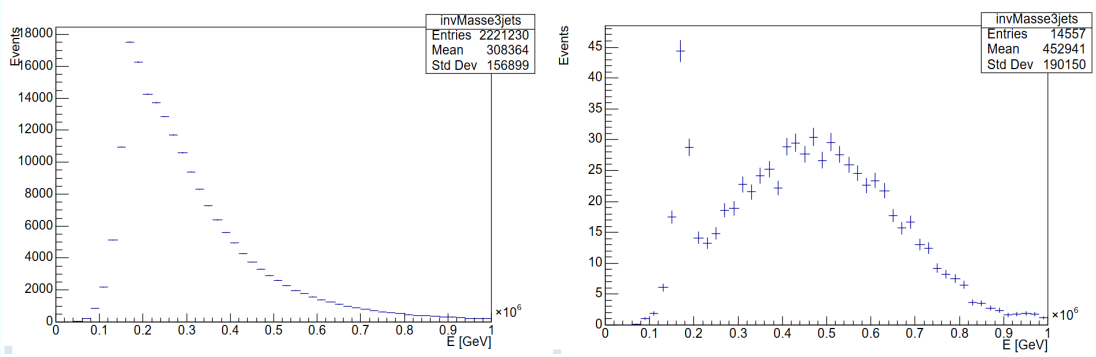

Figure 6: Reconstructed $t\bar{t}$ invariant 3 jet mass for SM $t\bar{t}$ (left) and Z' signal ($m_{Z'} = 1000\,\mathrm{GeV}$, right).

As an example of another high level observable, we have included the invariant mass constructed from three of the highest pT jets in the event. Although there is a difference the invariant mass of the 4 jet and lepton plus neutrino is the most physically motivated discriminatory variable.

2.3 Data–MC Agreement

Before performing a search for a resonance, it is essential to verify that the sum of all simulated background contributions reproduces the data in background-dominated

regions. This "data–MC agreement" check is implemented with `stackedPlots.C`, which produces so-called stack plots where each background process is drawn with a distinct fill color and the data points are overlaid (see Fig. 7).

Monte Carlo events are normalized to the dataset's integrated luminosity $\mathcal{L}$ and the theoretical cross section σ by applying the per-event weight

$$w = \frac{weight_{\mathrm{MC}} \times \mathcal{L} \times \sigma}{\sum_{\mathrm{gen}} weight_{\mathrm{MC}}},$$

where $\sum_{\mathrm{gen}} weight_{\mathrm{MC}}$ is the sum of generator weights before any selection. For data, $w = 1$. With this normalization, the integral of each MC histogram equals the expected yield for a perfect detector.

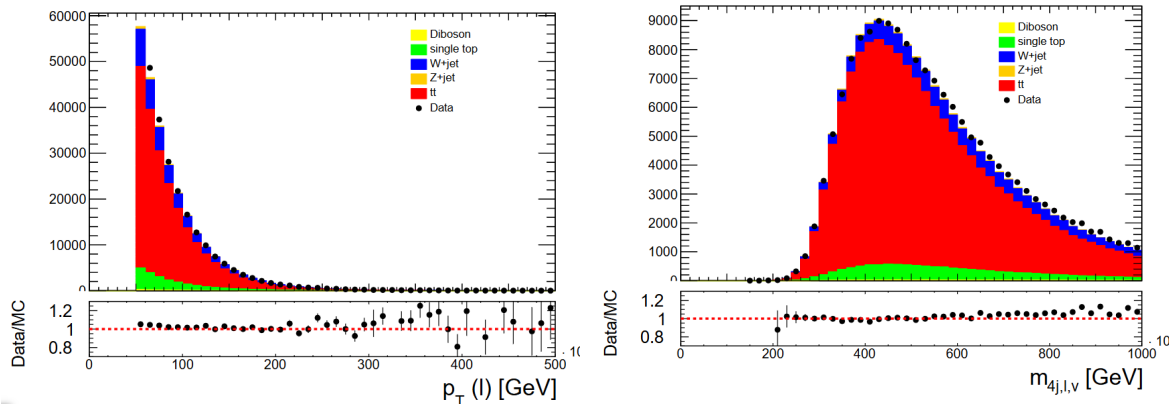

Figure 7: Stacked comparisons of (left) lepton p_T and (right) reconstructed $m_{t\bar{t}}$ between data and MC. The lower panel shows the data/MC ratio with statistical uncertainties.

Figure 7 demonstrates:

- **Lepton** p_T: Good overall shape agreement. Small deviations at high p_T ($>$ 200 GeV) remain within statistical uncertainties.
- $m_{t\bar{t}}$: The smoothly falling background sum matches data across the full mass range, with no significant local discrepancies.

To quantify agreement, we also use the provided `PlotStackWithRatio` function, which computes bin-by-bin data/MC ratios and displays them with error bars. Across all observables from Sec. 2.2.1 and the final discriminant from Sec. 2.2.2, the ratios fluctuate around unity with no coherent trend or outlying bins beyond ±20% (the size of our systematic uncertainties).
We therefore conclude that the background modeling is reliable in the control regions, and proceed to inspect the final $m_{t\bar{t}}$ spectrum for evidence of a signal. Just by looking at it, we do not see any indication of a signal. Here again, we do not include the many other figures produced during the analysis because they do not change or add anything to the conclusions of this section. This trend of no-signal by eye continues for all the observables studied.

3 Statistical Analysis

The final step of the search is a quantitative test of the data against the background-only hypothesis and, in absence of a significant signal, the derivation of exclusion limits on production.

3.1 Chi-Square Test

We use the provided `chiSquare.C` to compute the chi-square (χ^2) statistic between the observed data and the sum of all Standard Model backgrounds, bin by bin, in the distribution of the final discriminant $m_{t\bar{t}}$. After compiling:

```
make chiSquare
./chiSquare.exe
```

the program prints the total χ^2, the number of degrees of freedom (n.d.f.), and the corresponding p-value:

$$p = P(\chi^2,\, n.d.f.) \;=\; \int_{\chi^2}^{\infty} f_{\chi^2}(x;\, n.d.f.)\, dx.$$

A p-value below 2.7×10^{-3} (3σ) constitutes "evidence," while $p < 5.7 \times 10^{-7}$ (5σ) constitutes an "observation".

The interesting thing found here is that the p-value comes out to be $9.24088 \cdot 10^{-19}$ which would mean that we have stumbled upon a signal. Here, we have not included the systematic uncertainties which, as we will see now, change the result significantly.

3.2 Inclusion of Systematic Uncertainties

To assess the impact of experimental systematics, we repeat the χ^2 calculation with an additional flat uncertainty of 14% in each bin (combining 4% luminosity and an estimated 10% from sources such as b-tagging, lepton ID, etc.). The modified test statistic accounts for this by inflating each bin's variance:

$$\sigma^2_{\text{tot}} = \sigma^2_{\text{stat}} + (0.14 \times N_{\text{bkg}})^2.$$

We observe that the inclusion of systematic uncertainties typically increases the p-value, reducing the significance of any fluctuations. This time the p-value comes out to be 0.999. And any hopes of a new discovery is eliminated.

3.3 95% Confidence-Level Exclusion Limits

If no evidence or observation is claimed, we set upper limits on $\sigma(pp \to) \times \mathcal{B}(\to t\bar{t})$ at 95% CL. For each mass hypothesis m, we add a signal template to the background and vary its normalization until the χ^2 probability of data vs. (background+signal) drops below 0.05 (i.e. $1 - 0.95$). The resulting "observed" limit curve is plotted against the theoretical prediction:

Figure 8 illustrates the mass range in which a narrow signal is ruled out by this analysis at 95% CL.

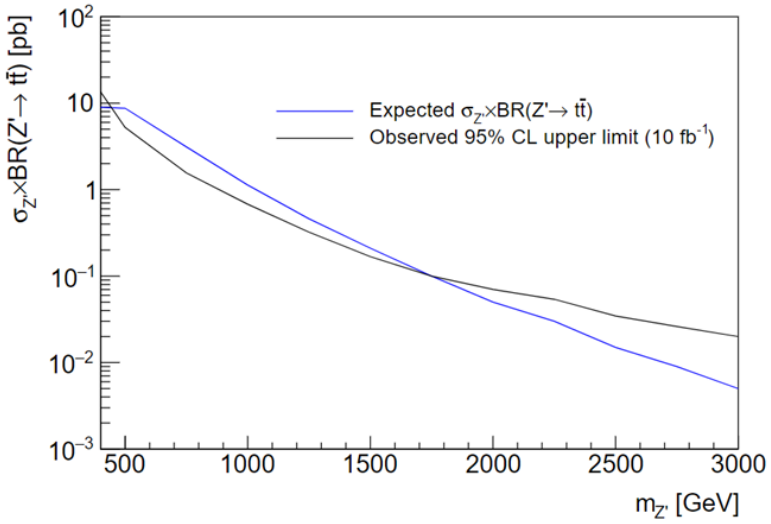

Figure 8: Observed 95% CL upper limits on $\sigma \times \mathcal{B}$ as a function of m, compared to the theoretical prediction. The region above the theory curve is excluded.

- **Expected limit (blue curve):** This is the median upper limit obtained under the background–only hypothesis, i.e. assuming no true Z' signal is present. It quantifies the analysis sensitivity to a narrow resonance of mass $m_{Z'}$ given statistical fluctuations of the Standard Model backgrounds.
- **Observed limit (black curve):** These points are the actual upper limits derived from the collision data. Any upward or downward fluctuation in the data relative to expectation will shift this curve above or below the expected limit, respectively.

Both axes use logarithmic scaling: the vertical axis spans roughly three orders of magnitude in $\sigma \times \mathcal{B}$, while the horizontal axis covers $m_{Z'}$ from 500 GeV to 3 TeV. As $m_{Z'}$ increases, parton luminosities decrease sharply, leading to weaker expected limits at high mass.

The close agreement between observed and expected limits over most of the mass range indicates no significant local excess or deficit in data. Small deviations (for example around 2 TeV) are consistent with statistical fluctuations well within the $\sim 1\sigma$ band.

Any theoretical model predicting $\sigma \times \mathcal{B}$ values above the black "observed" curve is excluded at 95 % CL. For instance, if a benchmark Sequential Standard Model Z' with $m_{Z'} = 1$ TeV predicts

$$\sigma \times \mathcal{B} \approx 0.5\ pb,$$

and the observed limit at 1 TeV is 0.4 pb, that model point would be ruled out by this analysis.

Finally, note that these limits are derived using an integrated luminosity of 10 fb^{-1} at $\sqrt{s} = 13$ TeV, demonstrating the power of even a moderate dataset to constrain heavy resonances.

4 Conclusion

In this study, we have carried out a search for a narrow $Z' \to t\bar{t}$ resonance in the lepton+jets channel using 1 fb^{-1} of $\sqrt{s} = 13$ TeV data collected by the ATLAS detector. Af-

ter applying a carefully optimized sequence of selection cuts (Section 2.1), we compared "low-level" kinematic observables—such as single-object p_T spectra—to "high-level" variables, and found that the reconstructed $t\bar{t}$ invariant mass $m_{t\bar{t}}$ offers the best separation power (Section 2.2.2). Background modeling was validated in multiple control regions (Section 2.3), and a binned χ^2 test of the $m_{t\bar{t}}$ distribution showed no significant deviation from the Standard Model expectation once systematic uncertainties were included (Section 3.2).

In the absence of a signal, we derived 95 % CL upper limits on $\sigma(pp \to Z') \times \mathcal{B}(Z' \to t\bar{t})$ as a function of $m_{Z'}$ (Section 3.3), excluding production rates above a few picobarns for masses up to 3 TeV. The observed limits closely follow the expected sensitivity, indicating that the data are well described by the background-only hypothesis (Figure 8).

Looking forward, several avenues could enhance the sensitivity of this search. Increasing the dataset to the full Run 2 luminosity (and beyond) would improve statistical reach, while advanced techniques—such as multivariate discriminants or boosted top quark reconstruction—could sharpen the separation between signal and background. Refinements in jet substructure algorithms and further reductions in systematic uncertainties (for example in b-tagging and jet energy calibration) will also be crucial. This exercise has provided us with a comprehensive exposure to the workflow of a modern resonance search, from trigger and object reconstruction through statistical interpretation, and lays the groundwork for future studies with larger datasets and more sophisticated analysis methods.

References

[1] ATLAS Collaboration. The ATLAS Experiment at the CERN Large Hadron Collider: A Description of the Detector Configuration for Run 3. *arXiv preprint*, May 2023.

[2] R. L. et al. Workman. Review of Particle Physics. *Progress of Theoretical and Experimental Physics*, 2022:083C01, 2022.

[3] ATLAS Collaboration. Top-Quark Public Results. https://twiki.cern.ch/twiki/bin/view/AtlasPublic/TopPublicResults. [accessed 09.10.2023].

[4] ROOT Development Team. ROOT — Data Analysis Framework. https://root.cern.ch.